Since January 2020 Elsevier has created a COVID-19 resource centre with free information in English and Mandarin on the novel coronavirus COVID-19. The COVID-19 resource centre is hosted on Elsevier Connect, the company's public news and information website.

Virus Research 163 (2012) 628–635

Contents lists available at SciVerse ScienceDirect

Virus Research

journal homepage: www.elsevier.com/locate/virusres

Coronavirus infection of rat dorsal root ganglia: Ultrastructural characterization of viral replication, transfer, and the early response of satellite cells

Yan-Chao Li[a,b], Wan-Zhu Bai[a,c], Norio Hirano[d], Tsuyako Hayashida[a], Tsutomu Hashikawa[a,*]

[a] Support Unit for Neuromorphological Analysis, RIKEN Brain Science Institute, Saitama 351-0198, Japan
[b] Department of Histology and Embryology, Norman Bethune College of Medicine, Jilin University, Changchun, Jilin Province 130021, China
[c] Institute of Acupuncture and Moxibustion, China Academy of Chinese Medical Science, Beijing 100700, China
[d] Department of Veterinary Microbiology, Iwate University, Morioka, Iwate 020-8550, Japan

ARTICLE INFO

Article history:
Received 1 November 2011
Received in revised form
26 December 2011
Accepted 28 December 2011
Available online 11 January 2012

Keywords:
Coronavirus
Dorsal root ganglia
Satellite cells
Virus propagation

ABSTRACT

Swine hemagglutinating encephalomyelitis virus (HEV) has been shown to have a capability to gain access to the cell bodies of sensory neurons after peripheral inoculation, resulting in ganglionic infection. It is not clearly understood how this virus is replicated within and released from the sensory neurons, and it remains to know how satellite cells response to the HEV invasion. By ultrastructurally examining HEV-infected rat dorsal root ganglia, we found that HEV in the cell bodies of infected neurons budded from endoplasmic reticulum–Golgi intermediate compartments, and were assembled either individually within small vesicles or in groups within large vesicles. The progeny virions were released from the sensory neurons mainly by smooth-surfaced vesicle-mediated secretory pathway, which occurred predominantly at the perikaryal projections and infoldings of sensory neurons. Released HEV particles were subsequently taken up by the adjacent satellite cells. Almost all virus particles in the cytoplasm of satellite cells were contained in groups within vesicles and lysosome-like structures, suggesting that these glial cells may restrict the local diffusion of HEV. These observations give some insights into the pathogenesis of coronavirus infection and are thought to help understand the interactions between sensory neurons and their satellite cells.

1. Introduction

Swine hemagglutinating encephalomyelitis virus (HEV) is a positive non-segmented, single-stranded RNA virus, belonging to Betacoronavirus together with mouse hepatitis virus, bovine coronavirus and human coronavirus OC43 (Masters, 2006; de Groot et al., 2012). As the first member of the group coronaviruses found to invade the central nervous system, HEV was initially isolated from encephalomyelitic piglet brains in 1960 by Greig et al. (1962) in Canada. Subsequent studies demonstrated that HEV first infected the epithelial cells lining the upper respiratory tract, and thereafter was delivered retrogradely via peripheral nerves to the central neurons in charge of peristaltic function of the digestive tracts, resulting in the so-called vomiting diseases (Andries and Pensaert, 1980; Yagami et al., 1986). In experimental animals, injection of HEV into rat hind footpad was reported to result in productive infection of the ipsilateral dorsal root ganglions (DRGs) and spinal cord at 3 day postinfection (p.i.), and productive infection of the contralateral primary motor cortex at day 4 p.i. (Hirano et al., 1993, 1998, 2004; Bai et al., 2008).

The cell bodies of the primary afferent neurons, which convey sensory information from the periphery to the central nervous system, are completely surrounded by several satellite cells (SCs). The unique structure of the SC envelope do not merely give mechanical or nutrient support to the neurons, but also enables SCs to exert a tight control of the extracellular microenviroment around the neurons (Hanani, 2005). So far, it is unclear how HEV is replicated in and transferred from the sensory neurons, and it remains to know what roles SCs play in the HEV-infected ganglia. Given that coronaviruses are able to make use of the cellular events preexisting in the host cells (for review, see Hobman, 1993; Masters, 2006), the clarification of the mechanism underlying coronavirus infection in the sensory ganglia was expected to help understand the cellular events in the ganglionic neurons as well as the relationship between the neurons and their SCs.

Previous experiments showed that HEV antigen-positive neurons appeared in DRGs at day 3 p.i., peaked in number at day 4 p.i., and declined thereafter (Hirano et al., 1998; Bai et al., 2008). At day

Abbreviations: HEV, swine hemagglutinating encephalomyelitis virus; DRG, dorsal root ganglia; SC, satellite cell; p.i., postinfection; ER, endoplasmic reticulum.

* Corresponding author at: Support Unit for Neuromorphological Analysis, RIKEN Brain Science Institute, Saitama 351-0198, Japan. Tel.: +81 48 467 5928; fax: +81 48 467 5926.
E-mail address: tom@brain.riken.jp (T. Hashikawa).

0168-1702/$ – see front matter © 2012 Elsevier B.V. All rights reserved.
doi:10.1016/j.virusres.2011.12.021

3 p.i., the neuronal-SC architecture remained almost intact, and SCs can be identified unequivocally by their morphology and perineuronal localization. Therefore, the DRGs collected at day 3 p.i. were used in this experiment in order to obtain detailed insights into the replication within and egress of HEV from infected neurons as well as the fine-structural changes of SCs at the early stage of infection.

2. Materials and methods

2.1. Virus, plaque assay and cell culture

HEV 67N strain was initially isolated from the nasal cavity of apparently healthy swine in Iowa, the U.S.A., during a routine survey for viruses harbored in the respiratory tract by Mengeling et al. (1972). This virus was originally obtained from Dr. W.L. Mengeling (National Animal Disease Laboratory, Ames, IA, USA), passaged 12 times in primary porcine kidney cell cultures (Hirai et al., 1974) and more than 10 times in suckling mouse brains by intracerebral inoculation. This mouse brain-adapted HEV 67N strain was plaque-purified 3 times in an established swine kidney cell line (Hirano et al., 1990), and thereafter was propagated 20 times in the same cell line until use.

The viral supernatant from infected cell culture, with a titer of 10^6 PFU/0.2 ml as assayed by plaque method, was kept at −80 °C, and used for all the experiments. Cell culture and plaque assay of the virus were carried out as described by Hirano et al. (1990).

2.2. Animals and virus inoculation

Eight male Wistar rats (4 weeks old, 70–90 g), specific pathogen-free and serologically negative for mouse hepatitis virus infections, were purchased from the SLC Company (Hamamatsu, Japan). Five rats were inoculated by injecting 200 μl of viral culture supernatant (10^6 PFU) subcutaneously in the right hind footpad with a 1 ml syringe under Halothane anesthesia (fluothane, Takeda Pharmaceutical Co. Ltd, Osaka, Japan). HEV-inoculated rats were reared separately in cages with food and water freely available. Three rats inoculated with virus-free cell culture supernatant were used as vehicle controls.

All the experiments with active virus were carried in a biosafety Level 2 facility containment, and performed in accordance with the Guide for the Care and Use of Laboratory Animals (National Academy Press, Washington, 1996).

2.3. Immunohistochemical detection of HEV antigen

Three days later, all the animals were anesthetized and perfused through the heart with 50 ml physiological saline, and followed by 200–300 ml of fixatives containing 2% glutaraldehyde and 2% tanic acid in 0.1 M phosphate buffer (pH, 7.4).

The L4 and L5 DRGs were dissected out, postfixed in fresh fixatives for 4–6 h, and then left in 0.1 M phosphate buffer containing 5% sucrose overnight at 4 °C. Sections of the ganglia were cut on about 50 μm thick a DSK microslicer (DTK-1000, ZERO-1, Dosaka EM, Kyoto, Japan). Parts of the serial sections were preincubtaed with normal horse serum containing 0.2% Triton X-100 for 30 min at room temperature and then incubated overnight at 4 °C with mouse anti-HEV antiserum (Hirano et al., 1990). After washes with 0.1 M phosphate buffer, sections were reacted with horse anti-mouse antibody conjugated to peroxidase (HRP, 1:500; Vector Labs, PI-2000) at room temperature for 1 h. The sections were then incubated with 0.02% 3,3′-diaminobenzidine tetrahydrochloride (Sigma, St. Louis, MO) in 50 mM Tris-buffer containing 0.01% H_2O_2. The specificity of the primary antibody has been reported previously (Hirano et al., 1990), and was verified by replacing the antiviral serum with 0.1 M phosphate buffer in this study. Stained sections were observed using a light microscope equipped with a digital camera (Eclipse; Nikon Co., Tokyo, Japan).

2.4. Transmission electron microscopy

The remaining sections were fixed in 1% osmium tetroxide in 0.1 M phosphate buffer (pH 7.4) for 2 h at 4 °C, dehydrated in increasing concentrations of ethanol and embedded in Epon 812.

Ultrathin sections about 80 nm thick were cut on an ultracut E ultramicrotome (Reichert-Jung, Wien, Austria), and collected on Formvar-coated slots. The ultrathin sections were stained with uranyl acetate and lead citrate, and then examined with a transmission electron microscope (TECHNAI 12 FEI, OR, USA).

High-resolution electron micrographs were recorded on Image Plates (FujiFilm, Tokyo, Japan), which were scanned with Fujifilm FDL 5000 and converted into digital images with a software Image gauge V4.0 (FujiFilm, Tokyo, Japan).

The dimensions of virus particles and virus-containing vesicular structures were measured at a magnification ×30,000 on electron micrographs with a software Olympus Soft Imaging Solutions GmbH (version 1.2, Münster, Germany).

3. Results

In 4-week-old rats inoculated subcutaneously in the hind footpad, HEV antigen was detected initially at day 3 p.i. in the lumbar ganglia on the ipsilateral side. Positive neurons were scattered throughout the ganglia, ranging in diameter from 25 to 60 μm (Fig. 1). Among them, about 80% showed a mediate to large size (30–50 μm in diameter).

HEV-infected neurons of various sizes were examined by electron microscopy for ultrastructural localization and analysis of virus particles. Since no apparent differences were found between different neuronal groups in our preparations, the results were presented together for the convenience of description.

3.1. Replication and assembly of HEV in the DRG neurons

Under the electron microscope, HEV particles in infected DRG neurons were identified as spherical particles inside vesicles or as electron-dense materials in the process of budding into the intracellular membranous cisternae (Figs. 2 and 3), as described previously (Clarke and McFerran, 1971; Mengeling et al., 1972;

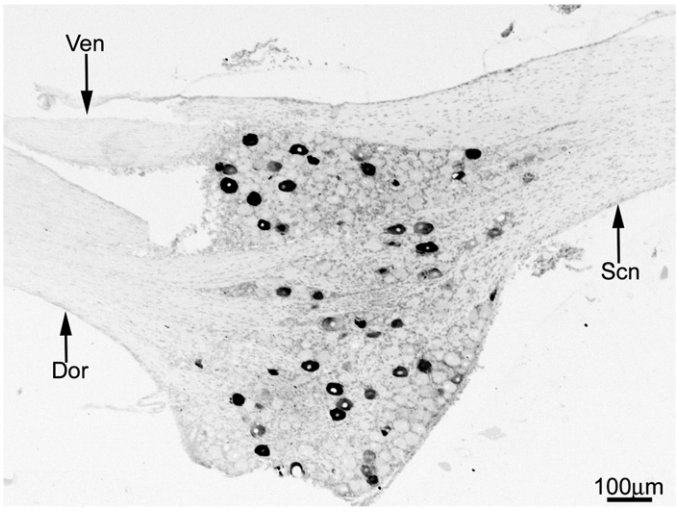

Fig. 1. HEV antigen in the DRG. Scale bar: 100 μm. A representative light micrograph shows the immunohistochemical distribution of HEV antigen in a longitudinally cut DRG. Dor: dorsal root; Ven: ventral root; Scn: sciatic nerve.

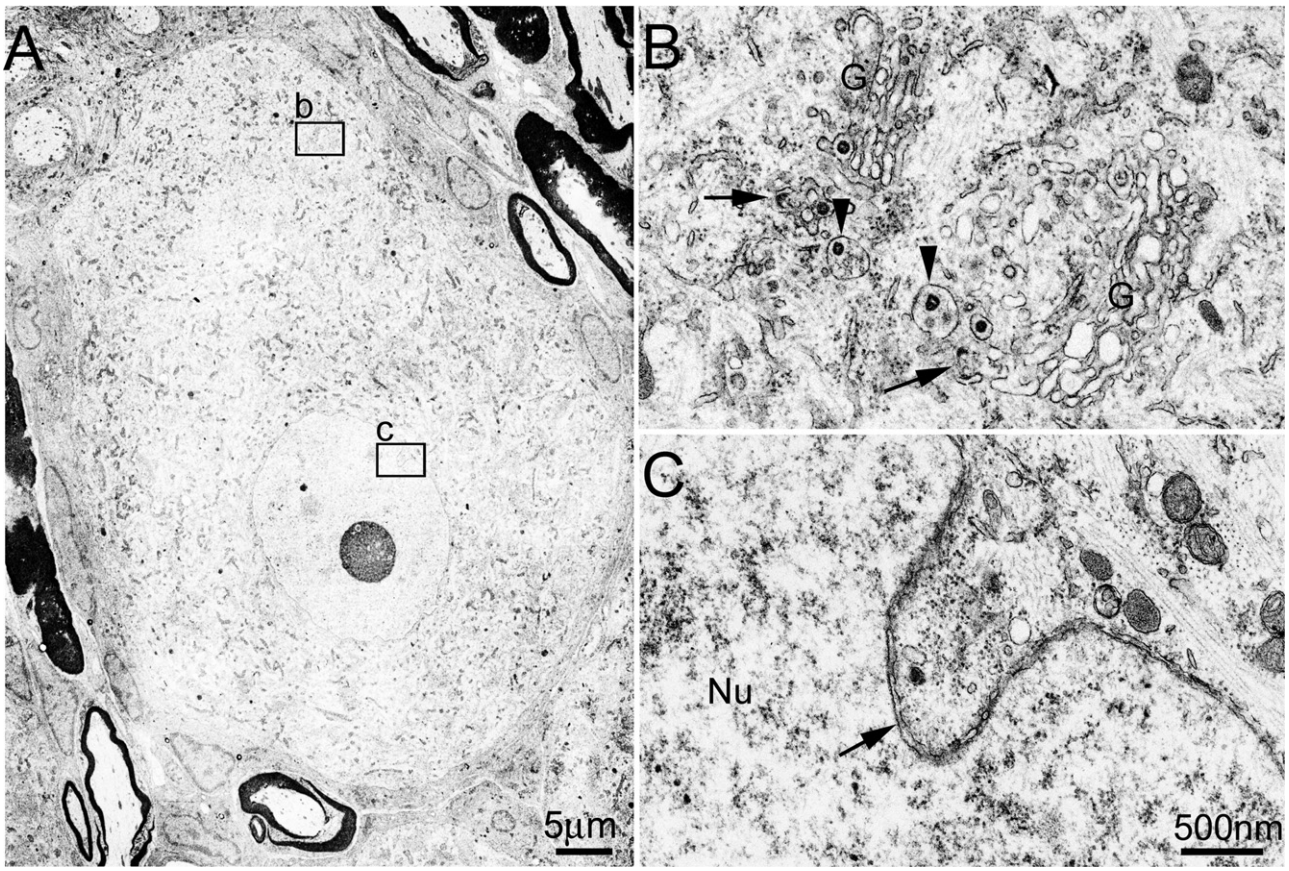

Fig. 2. Morphogenesis of HEV in the DRG neuron. Scale bars: A, 5 μm; B and C, 500 nm. Panel A shows an HEV-infected DRG neuron. The details in insets b and c are given in panels B and C, respectively, showing that morphogenesis of HEV occurs exclusively in the perikaryal cytoplasm. In panel B, viral budding profiles (arrows) can be observed in ER and in the lateral rims of Golgi complexes (G). Besides small vesicles enclosing single virions, large vesicles (arrowheads) containing more than one virion are also found in the Golgi areas. No virus-related structures are seen within the nucleus (C), but nuclear envelope invaginations are often encountered (arrow).

Yagami et al., 1986). Progeny virions had an electron-lucent or dense center, and ranged in diameter from 65 to 116 nm (73.4 ± 12.1 nm, mean ± SEM, $n = 55$). The outer surfaces of the viral envelopes were sometimes covered by a layer of well-defined projections, forming a typical "corona" profile (see the inset in Fig. 3D). As control, no similar structures were found in the samples from vehicle-inoculated animals (Fig. 4).

HEV particles in infected DRG neurons were observed exclusively in the cytoplasm, but not in the nucleus (Fig. 2). The earliest viral assembly that could be distinguished inside infected neurons was an electron-dense crescent segment indenting into the external membrane of endoplasmic reticulum (ER) or Golgi cisternae in the perikaryal cytoplasm (Figs. 2B and 3A). Large crescent segments were observed bulging into the lumen of ERs by incorporating the ER membrane (arrows in Fig. 3A). Virus particles were also found within the dilated lateral rims of the Golgi complexes (arrowheads in Fig. 3B).

A small number of progeny virions were enclosed individually within small vesicles in the trans-Golgi networks (Fig. 3C). These vesicles ranged from 90 to 180 nm in diameter, and a few of them were covered with small spinule coats around the outer surface (arrow in Fig. 3C). The membranous decorations were about 15–20 nm long, and were also noted on parts of trans-Golgi networks as well as some small empty vesicles in the cytoplasm (arrowheads in Fig. 3C).

By contrast, the majority of virus particles were contained in groups within large cytoplasmic vesicles, which ranged in diameter from 114 nm to 697 nm (299.0 ± 116.1, mean ± SEM, $n = 60$). These smooth-surfaced vesicles were distributed throughout the cytoplasm of infected neurons, but often observed in the Golgi areas and beneath the cell surface (Figs. 2B, 3B, 3D, 5D and 5F). Some vesicles showed increased electron density, and were derived apparently from smaller vesicles by fusion with each other (arrows in Fig. 3D). In uninfected neurons, intracellular vesicles of varying size were frequently encountered, but virus-like particles were never found within them (Fig. 4).

3.2. HEV egress from the DRG neurons

At least two ways of virus egress were found to occur at the cell surface of infected DRG neurons, one mediated by coated vesicles and the other by large smooth-surface vesicles.

As described above, virus-containing coated vesicles, with one virion within one vesicle, were occasionally observed in the cytoplasm of infected neurons. In this case, HEV particles could be released extracellularly by fusion of the coated membrane with the plasma membrane of the neurons, as shown in Fig. 5A. As a rule it was not possible to judge the direction of movement for vesicles opening onto the cell surface. Although in some cases the extracellular virus particles were surely those librated from the infected neurons because no HEV particles were found in the adjacent SCs (for example, Fig. 5B), the possibility could not be excluded that the already released virions may re-enter into the host neurons in a secondary cycle of infection. However, even so, the coated vesicles were certain to play a pivotal role in the process of HEV transfer.

By contrast, the majority of progeny virions were present in groups within smooth-surfaced vesicles in the cytoplasm of infected neurons. These large vesicular structures were also

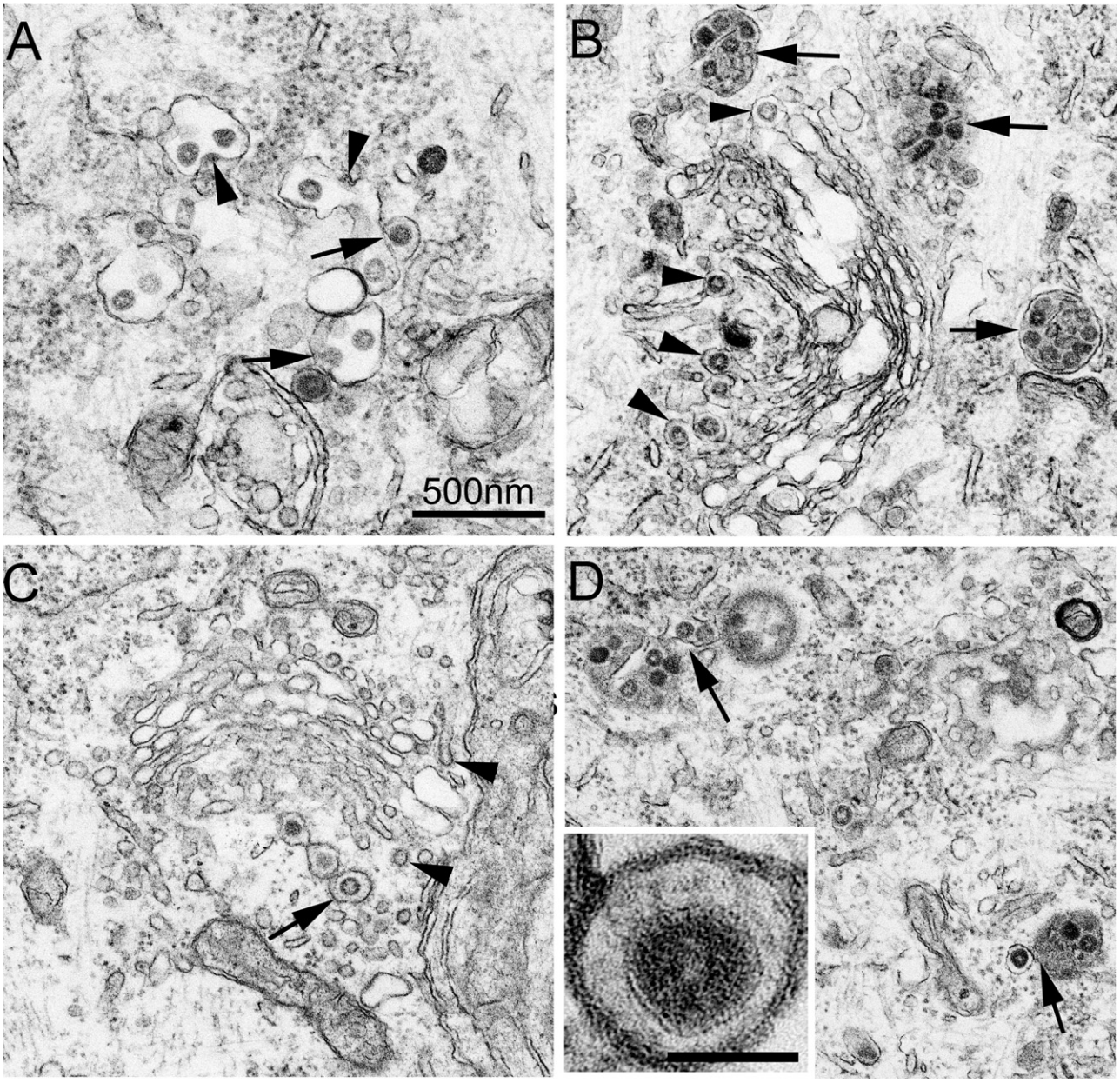

Fig. 3. The replication and assembly of HEV in the DRG neurons. Scale bar: 500 nm. Panel A shows the budding profiles of HEV at different stages in the ER areas. Arrowheads indicate electron-dense crescent segments attached to the external membrane of ER cisternae, while arrows indicate larger crescent segments that have bulged into the lumen of ER cisternae. Panel B shows groups of virions enclosed within large smooth-surfaced vesicle (arrows) in the Golgi areas. The arrowheads indicate virus particles present in the dilated rims of the trans-Golgi network. Panel C shows progeny virions enclosed individually within small vesicles in a trans-Golgi network. The arrow indicates a coated vesicle containing a single virion. Similar coating structures are also present on a small empty vesicle as well as part of the trans-Golgi networks (arrowheads). Panel D shows that virus-containing vesicles are attached to each other (arrows). The inset in panel D is a high-power electron micrograph, showing a virus enclosed within a vesicle. A layer of surface projections can be seen surrounding the viral envelope beneath the vesicle membrane.

observed beneath the cell surface, where they liberated virus particles out of the neurons mainly by way of neuronal projections (Fig. 5C–F). In single sections, neuronal projections were sometimes found as finger-like structures arising from the perikaryon of DRG neurons (Fig. 5C and D), but more often they were embedded within the cytoplasm of SCs appearing as an electron-lucent structure surrounded by two layers of plasma membranes (Fig. 5E and F). Virus particles were contained within smooth-surfaced vesicles in the cytoplasm of the neuronal projections (Fig. 5C–E). The intercellular space between neuronal cell bodies and their SCs, which were generally narrow with a distance of about 20 nm (Fig. 4), became abnormally enlarged at the sites where virus egress occurred (Fig. 5D–F). Large numbers of virus particles were accumulated outside along the plasma membrane of infected neurons, and surrounded by the adjacent SCs (Figs. 5D–F and 6A).

In addition, HEV egress was also observed to occur by way of neuronal infoldings, which were formed due to the plasma membrane invaginations. Such perikaryal specializations varied in depth, and their cytoplasmic sides were often closely contacted with subsurface cistern-like structures (arrowheads in Fig. 6A).

3.3. The early response of SCs

Infected neurons surrounded by uninfected SCs were observed, but the converse was not true, implying that the neuron was the

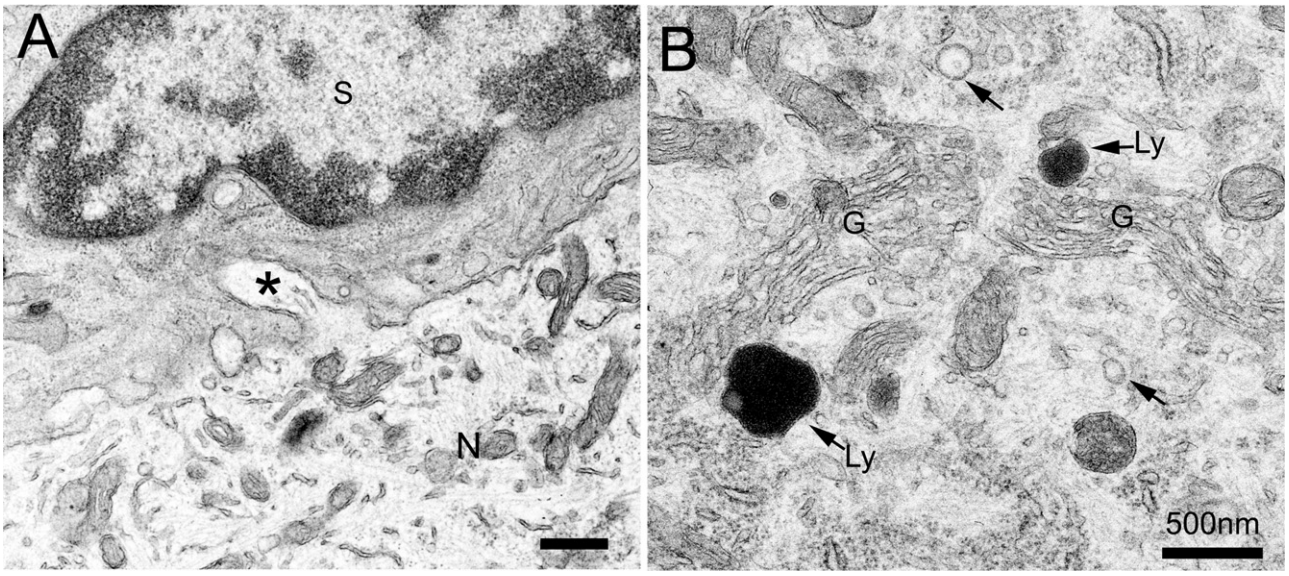

Fig. 4. Electron microphotographs from the vehicle controls. Scale bars: 500 nm. A: No virus particles are seen in either the neurons (N) or the surrounding SCs (S). The intercellular space between neuronal cell bodies and their SCs are generally narrow with a distance of about 20 nm. The neuronal-SC boundary is complicated by the presence of numerous projections, which arose from either the neuron or the adjacent SCs. The neuronal projections occur more frequently. In single sections, they are sometimes seen continuous with the neuronal cell surface (asterisk). B: In the neurons, lysosomes (labeled arrows) and vesicles (arrows) of varying size are frequently located near the Golgi apparatuses (G). No virus particles are found within the vesicles or the lysosome-like structures.

cell initially infected in the DRG. Immune cell infiltration was not apparent in the samples collected at the early stage of infection. The SCs adjacent to infected neurons remained largely unchanged, and could be easily distinguished by their peri-neuronal localization. These cells were invested with an outer capsule of connective tissue, and possessed a round, oval or flattened nucleus with both peripherally and centrally located clumps of chromatin (Fig. 6).

Almost all virus particles in the cytoplasm of SCs were contained in groups within vesicles (Figs. 5 and 6). Some virus-containing vesicles were located in the proximity of the perikaryal specializations of DRG neurons (for example, arrowhead in Fig. 5F). In this case, some of them may be parts of extracellular structures, since extracellular virus particles surrounded with the plasma membrane of SCs had a similar appearance in transverse sections.

Virus-containing vesicles were noted in the cytoplasm of the SCs away from the site of HEV egress (Figs. 5D and 6A). Moreover, virus particles in the SCs were found within lysosome-like structures (Figs. 5A and 6B), which were different from virus-containing extracellular portions in both morphology and electron density.

On the other hand, single enveloped virions were not observed, nor were viral profiles found in the SCs.

4. Discussion

In infected DRGs, the replication of HEV occurred exclusively in the cytoplasm of sensory neurons. The virus particles of HEV showed morphological characteristics similar to those already described for the same (Mengeling et al., 1972; Yagami et al., 1986) or different HEV strains (Clarke and McFerran, 1971; Ducatelle et al., 1981). HEV were found to bud from endoplasmic reticulum–Golgi intermediate compartments, and assemble through Golgi complexes with the resultant progeny virions enclosed either individually within small vesicles or in groups within large vesicles.

The evidence accumulated so far suggested that coronavirus egress is accomplished mainly by use of the constitutive exocytic pathway (for review, see Hobman, 1993; Masters, 2006). Studies on mouse hepatitis virus and transmissible gastroenteritis virus in cultivated cells have showed that progeny virions were collected in groups within one large vesicle lacking clathrin coats, transported along the constitutive exocytic route to the host cell surface, and liberated by the fusion of the vesicle membrane with the plasma membrane (Tooze et al., 1987; Salanueva et al., 1999).

By contrast, some coronaviruses such as infectious avian bronchitis virus (beaudette strain) have been reported able to get out of the host cells by coated vesicle-mediated exocytosis (Chasey and Alexander, 1976). Previous electron microscopic data suggested that HEV seemed to be released in groups from cultured porcine kidney cells by way of smooth-surfaced vesicles (Clarke and McFerran, 1971). However, in vivo data on HEV transfer are still not available. In the present study we showed that HEV progeny virions can get out of DRG neurons by either of the means described above, but mainly by the large smooth-surfaced vesicle-mediated pathway.

An important finding in the present study was that the large vesicle-mediated egress of HEV occurred preferably at the perikaryal projections and infoldings of DRG neurons. The roles of these perikaryal specializations during HEV infection seem to require further investigations. At the release sites, HEV particles were accumulated in the dilated extracellular space between the neurons and their SCs, and subsequently taken up within vesicular structures by the SCs. Viral replication signs were absent in the cytoplasm of the SCs. On the other hand, the presence of virus particles within lysosome-like structures in the SCs as well as the disappearance of virus particles in the later stage (data not shown) indicated that HEV seemed to be finally cleared by these cells. These observations suggested that SCs may play a restrictive role during HEV propagation.

SCs have long been regarded as nursing cells involved in the maintenance of sensory neuron homeostasis by regulating extracellular ion and nutrient levels within sensory ganglia. On the other hand, increasing evidence showed that SCs can function as phagocytes to clear the cell debris of degenerative neurons during neural traumas (Tay et al., 1984a,b; Zhang et al., 1994) and viral infections (Alemañ et al., 2001). Moreover, the SCs resident in human trigeminal ganglia have recently been shown to closely

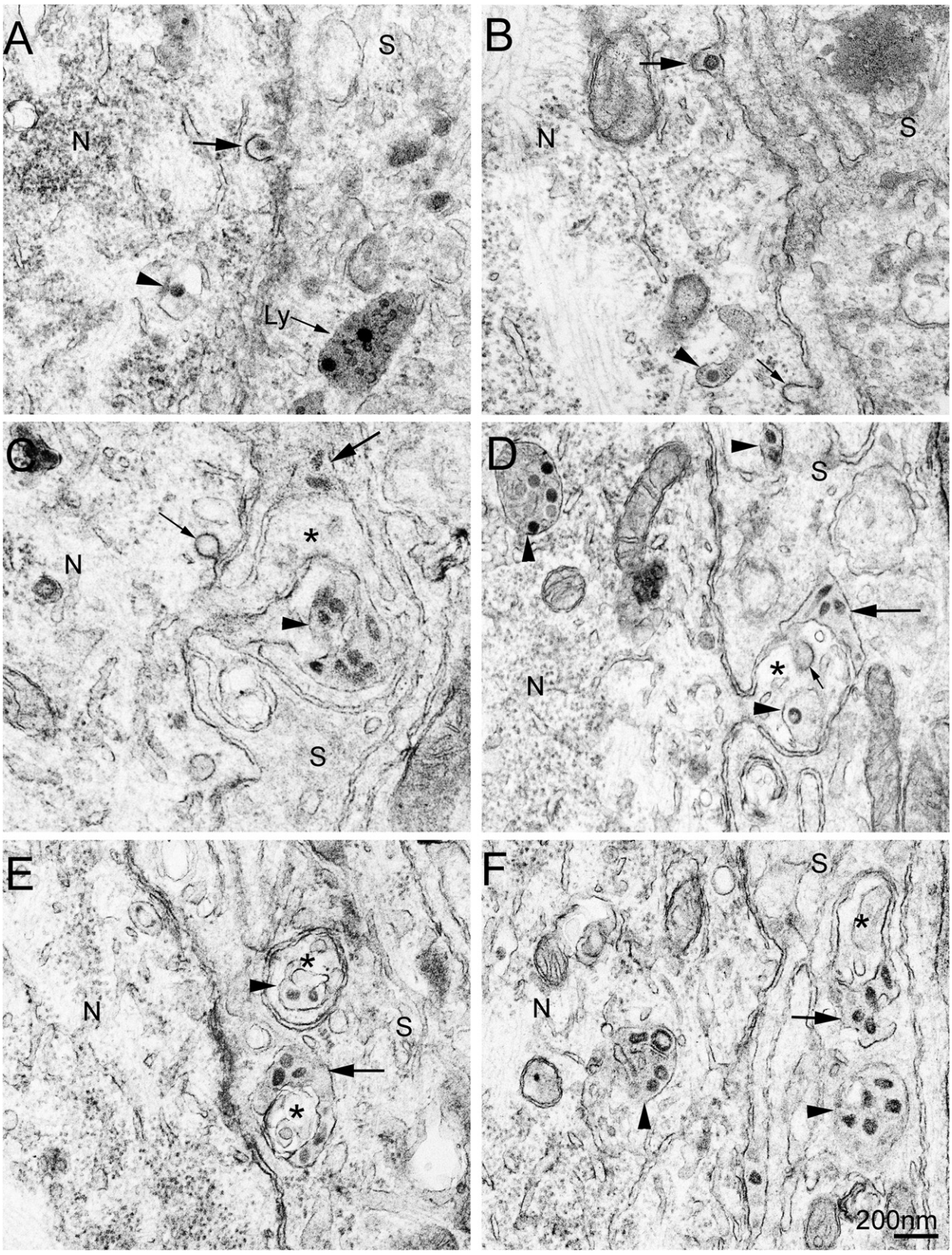

Fig. 5. HEV transfer between DRG neurons and their SCs. Scale bar: 200 nm. Neurons (N) and SCs (S) are marked in all images. Arrowheads indicate virus-containing vesicular structures in the cytoplasm of neurons or SCs. Large arrows indicate extracellular virus particles between the neuronal cell bodies and their SCs. Small arrows indicate empty coated vesicles or invaginations. Top row panels show coated vesicle-mediated HEV transfer. Panel A shows a coated vesicle containing a single virion fusing with the plasma membrane of an infected neuron. A lysosome-like structure (arrow labeled by Ly), which contains several virus-like particles, is found in the cytoplasm of the adjacent SCs. Panel B shows a virion located extracellularly between an infected neuron and its SC, where the invaginated plasma membrane of the infected neuron is covered with a layer of coating decorations (larger arrow). Panels in middle and bottom rows show HEV transfer by use of large smooth-surface vesicles, which is found to occur in neuronal perikaryal specializations. In Panels C and D, the neuronal projections are seen arising from the neuronal cell body and appear as microvillus-like structures (asterisks). Panels E and F show cross-sectioned neuronal projections (asterisks), which are embedded within the cytoplasm of SCs without continuity with the neuronal cell bodies.

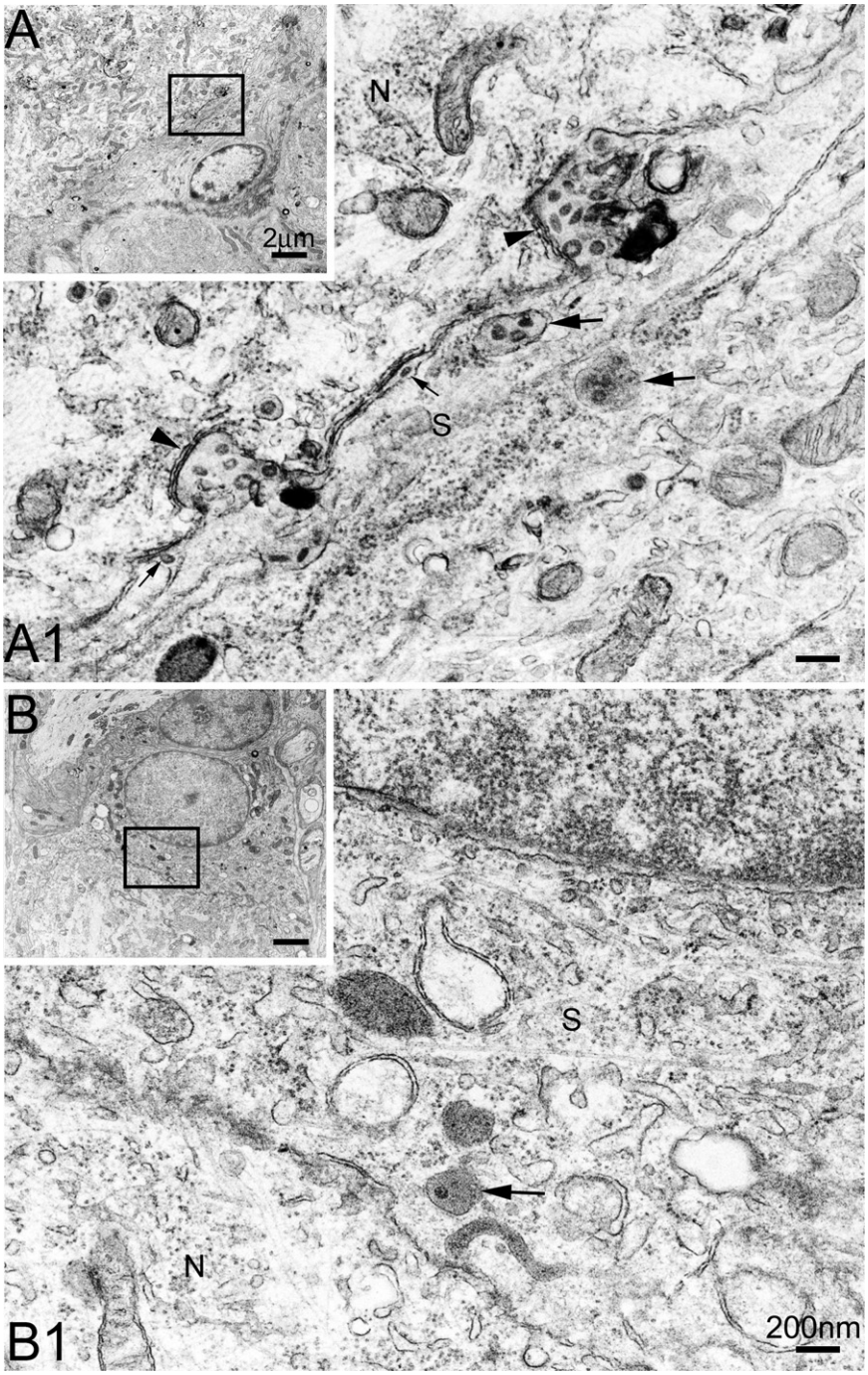

Fig. 6. HEV transfer and the reactions of SCs. Scale bars: A and B, 2 μm, A1 and B1, 200 nm. Neurons (N) and SCs (S) are marked in all images. Panel A shows the boundary of an infected neuron and its SC. Details of the inset are shown in panel A1 under higher magnification. Numerous virions are distributed extracellularly near infolded cell surface of the infected neuron, where subsurface cisternae are seen closely attached to the invaginated plasma membrane on the cytoplasmic side (arrowheads). A few virions (small arrows) are also noted in the narrow extracellular space along smooth parts of the neuronal cell surface. In the cytoplasm of the SC, there are many vesicles (large arrows) containing groups of virus particles. Panel B shows a SC adjacent to an infected neuron. Details of the inset are shown in panel B1 under higher magnification. HEV particles present in the SC are located within lysosome-like structures (arrow), but no single virions or viral budding profiles are found.

resemble microglia because they have also phenotypic and functional antigen-presenting cell properties (van Velzen et al., 2009). Our results showed that SCs engulfed only the released virions but not the cell bodies of HEV-infected neurons at the early stage of HEV infection. This form of phagocytosis does not resemble traditional SC phagocytosis of degenerating or apoptotic neurons. Given that coronaviruses are able to make use of the cellular events pre-existing in the host cells (for review, see Hobman, 1993; Masters, 2006), it is of interest to know whether a similar scavenging mechanism can be used by SCs under normal conditions to control the microenvironments surrounding the subjacent neurons.

As far as we know, this is the first report that has in detail examined the coronavirus infection in the sensory ganglia. By examining HEV-infected DRG, we disclosed several morphologic details about HEV assembly and propagation in the ganglia, which is thought to help understand the mechanism underlying coronavirus infection and give some insights into the interactions between sensory neurons and their SCs.

References

Alemañ, N., Quiroga, M.I., López-Peña, M., Vázquez, S., Guerrero, F.H., Nieto, J.M., 2001. Induction and inhibition of apoptosis by pseudorabies virus in the trigeminal ganglion during acute infection of swine. J. Virol. 75, 469–479.

Andries, K., Pensaert, M.B., 1980. Immunofluorescence studies on the pathogenesis of hemagglutinating encephalomyelitis virus infection in pigs after oronasal inoculation. Am. J. Vet. Res. 41, 1372–1378.

Bai, W.Z., Li, Y.C., Hirano, N., Tohyama, K., Hashikawa, T., 2008. Transneuronal infection and associated immune response in the central nervous system induced by hemagglutinating encephalomyelitis virus following rat hindpaw inoculation. Neurosci. Res. 61 (Suppl. 1), S135.

Chasey, D., Alexander, D.J., 1976. Morphogenesis of avian infectious bronchitis virus in primary chick kidney cells. Arch. Virol. 52, 101–111.

Clarke, J.K., McFerran, J.B., 1971. An electron microscopic study of haemagglutinating encephalomyelitis virus of pigs. J. Gen. Virol. 13, 339–344.

Ducatelle, R., Coussement, W., Hoorens, J., 1981. Morphogenesis of hemagglutinating encephalomyelitis virus (HEV) in vivo and in vitro. Vlaams Diergeneeskundig Tijdschrift 50, 326–336.

de Groot, R.J., Baker, S.C., Baric, R., Enjuanes, L., Gorbalenya, A., Holmes, K.V., Perlman, S., Poon, L., Rottier, P.J.M., Talbot, P.J., Woo, P.C.Y., Ziebuhr, J., 2012. Coronaviridae. In: King, A.M.Q., Adams, M.J., Carstens, E.B., Lefkowitz, E.J. (Eds.), Virus Taxonomy, Classification and Nomenclature of Viruses, Ninth Report of the International Committee on Taxonomy of Viruses. International Union of Microbiological Societies, Virology Division. Elsevier Academic Press, Waltham, MA, USA, pp. 806–828, ISBN: 978-0-12-384684-6.

Greig, A.S., Mitchell, D., Corner, A.H., Bannister, G.L., Meads, E.B., Julian, R.J., 1962. A hemagglutinating virus producing encephalomyelitis in baby pigs. Can. J. Comp. Med. Vet. Sci. 26, 49–56.

Hanani, M., 2005. Satellite glial cells in sensory ganglia: from form to function. Brain Res. Brain Res. Rev. 48, 457–476.

Hirai, K., Chang, C.N., Shimakura, S., 1974. A serological survey on hemagglutinating encephalomyelitis virus infection in pigs in Japan. Nippon Juigaku Zasshi 36, 375–380.

Hirano, N., Haga, S., Fujiwara, K., 1993. The route of transmission of hemagglutinating encephalomyelitis virus (HEV) 67N strain in 4-week-old rats. Adv. Exp. Med. Biol. 342, 333–338.

Hirano, N., Nomura, R., Tawara, T., Tohyama, K., 2004. Neurotropism of swine haemagglutinating encephalomyelitis virus (coronavirus) in mice depending upon host age and route of infection. J. Comp. Pathol. 130, 58–65.

Hirano, N., Ono, K., Takasawa, H., Murakami, T., Haga, S., 1990. Replication and plaque formation of swine hemagglutinating encephalomyelitis virus (67N) in swine cell line, SK-K culture. J. Virol. Methods 27, 91–100.

Hirano, N., Tohyama, K., Taira, H., 1998. Spread of swine hemagglutinating encephalomyelitis virus from peripheral nerves to the CNS. Adv. Exp. Med. Biol. 440, 601–607.

Hobman, T.C., 1993. Targeting of viral glycoproteins to the Golgi complex. Trends Microbiol. 1, 124–130.

Masters, P.S., 2006. The molecular biology of coronaviruses. Adv. Virus Res. 66, 193–292.

Mengeling, W.L., Boothe, A.D., Ritchie, A.E., 1972. Characteristics of a coronavirus (strain 67N) of pigs. Am. J. Vet. Res. 33, 297–308.

Salanueva, I.J., Carrascosa, J.L., Risco, C., 1999. Structural maturation of the transmissible gastroenteritis coronavirus. J. Virol. 73, 7952–7964.

Tay, S.S., Wong, W.C., Ling, E.A., 1984a. An ultrastructural study of the non-neuronal cells in the cardiac ganglia of the monkey (Macaca fascicularis) following unilateral vagotomy. J. Anat. 138, 411–422.

Tay, S.S., Wong, W.C., Ling, E.A., 1984b. An ultrastructural study of the neuronal changes in the cardiac ganglia of the monkey (Macaca fascicularis) following unilateral vagotomy. J. Anat. 138, 67–80.

Tooze, J., Tooze, S.A., Fuller, S.D., 1987. Sorting of progeny coronavirus from condensed secretory proteins at the exit from the trans-Golgi network of AtT20 cells. J. Cell Biol. 105, 1215–1226.

van Velzen, M., Laman, J.D., Kleinjan, A., Poot, A., Osterhaus, A.D., Verjans, G.M., 2009. Neuron-interacting satellite glial cells in human trigeminal ganglia have an APC phenotype. J. Immunol. 183, 2456–2461.

Yagami, K., Hirai, K., Hirano, N., 1986. Pathogenesis of haemagglutinating encephalomyelitis virus (HEV) in mice experimentally infected by different routes. J. Comp. Pathol. 96, 645–657.

Zhang, Y.L., Tan, C.K., Wong, W.C., 1994. An ultrastructural study of the ciliary ganglia of cat and monkey (Macaca fascicularis) following section of the short ciliary nerves. J. Anat. 185, 565–576.